Indian Journal of Pure & Applied Physics
Vol. 54, November 2016, pp. 701-712

Modeling of glow discharge in dielectric barrier

Mankour Mohamed[a]*, Hartani Kada[a] & Belarbi Ahmed Wahid[b]

[a]Electrotechnical Engineering Laboratory, University Tahar Moulay of Saida, Algeria
[b]Department of Electechnical, Faculty of Electrical Engineering, University of Sciences and Technology of Oran, Algeria

Received 1 March 2016; revised 22 August 2016; accepted 2 September 2016

Numerical calculations of spatio-temporal characteristics of the homogeneous dielectric barrier discharge (DBD) in pure helium have been performed by means of a one-dimensional fluid model. The influence of the elementary processes on the discharge behavior has been studied by variation of the corresponding rate constants. The simulation and the analytical interpretation have been carried out for two basic modes of the homogeneous barrier discharge. The specificity of the glow discharge is the development of a cathode region and a positive column during the breakdown, as well as the presence of quasi-neutral plasma in subsequent phases. The positive column occurs because the shielding of the external field by the plasma is not instantaneous. The dependence of the discharge behavior on the external parameters, such as, the amplitude and frequency of the applied voltage, discharge gap width and thickness of dielectric barriers has been analyzed.

Keywords: Glow discharge DBD, Fluid model, Helium gas, Dielectric barriers

1 Introduction

The atmospheric pressure gas discharges is the subject of interest in recent years because of their application in industrial plasma technologies, such as, surface treatment and plasma chemistry[1-3]. The dielectric barrier discharge (DBD) is a low-frequency ac discharge between two plane electrodes covered by a dielectric barrier.

In recent years many studies have been concerned with the effects of gas flow and electrode geometry on the discharge mode and characteristics. While several authors have published experimental and modeling studies of plane-parallel DBD at atmospheric pressure, under specific conditions, for instance, at least one of electrodes covered with a dielectric layer, an ac power with an appropriate frequency, etc., atmospheric pressure glow discharges (APGD) is obtained relatively readily in helium. Helium APGD has been studied extensively. For simplicity, many theoretical studies made an approximation that the average electron energy is constant throughout the discharge space at any time; the value of electron energy is chosen empirically.

The line of works in the glow discharge with dielectric barrier is to turn towards a very detailed modeling of the discharge. A good modeling makes it possible to understand and predict their behavior[4–12]. The control and use of this technology is used for industrial needs, such as semi-conductors, panels of plasma visualization, the deposit of the thin layers, the die-sinking in micro-electronics and the treatment of surfaces[13–17].

APGD can be used not only for surface modification but also for many other applications such as gas transformation (depollution), thin film deposition and dry etching. It is of paramount importance to determine their stability conditions very carefully and to study the transition between APGD and DBD. It is obvious that to reach a better understanding of the mechanisms of these discharges and to optimize their parameters.

2 Physical Models

2.1 Parallel plate dielectric barrier configuration

Let us consider a parallel at plate electrodes discharge geometry and the dielectric barriers are attached with the electrodes as shown in Fig. 1.

A sinusoidal voltage is imposed on the driven electrode and the other electrode is grounded. The front dielectric barrier surfaces, i.e., ABCD and EFGH are directly linked with the discharge plasma in the positive and negative half cycles of sinusoidal input voltage. The dielectric barriers have smaller widths as compared to the gap width. The combination of d1 and d2 represents the area of cross section (d1_d2) for the incoming gas, while the coordinates x, y and z represent the three-dimensional geometrical arrangement[18-20].

*Corresponding author (E-mail: mankourmohamed312@yahoo.fr)

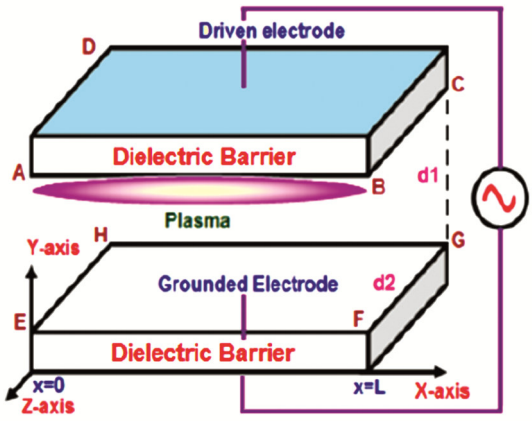

Fig. 1 — Parallel plate dielectric barrier in the presence applied sinusoidal voltage

Table 2 — Definition of constants and coefficients for simulation[34]

Parameter	Symbol	Value
Electron mobility	μ_e	987 $cm^2/(V.s)$
Ion mobility	μ_i	14 $cm^2/(V.s)$
Neutral density	n_0	$2.5.10^{19}$ cm^{-3}
Pollutant density	n_p	Adjusted
Penning ionization rate	k_{pm}	$5x10^{-10}$ cm^3s^{-1}
Radiative recombination rate	k_m	$7x10^5$ s^{-1}
Three body recombination rate	k_{2m}	$2.5x10^{-34}$ cm^6s^{-1}
Secondary emission yield	γ_i	0.1
Metastable diffusion coefficient	D_m	0.6 cm^2s^{-1}
Ion diffusion coefficient	D_i	0.354 cm^2s^{-1}
Electron diffusion coefficient	D_e	Function
Excitation coefficient	α_{ex}	Function
Ionization coefficient	α_{io}	Function
Electric field	E	Function
Stepwise ionization coefficient	k_{em}	Function

Table 1 — Fast processes in helium (He) plasmas[21-27]

Process	Notation	Rate constant
Associative ionization	$H_e^* (n \geq 3) + H_e \rightarrow H_{e2}^+ + H_e$	1.5×10^{-11} cm^3/s
H_e^+ conversion	$H_e^+ + 2H_e \rightarrow H_{e2}^+ + H_e$	1.1×10^{-31} cm^6/s
Conversion of resonance atoms	$H_e(2^3P) + 2H_e \rightarrow H_{e2}(A^1\sum_u^+) + H_e$	1.6×10^{-32} cm^6/s
Excimer radiation	$H_{e2}(b^3\pi_g) \rightarrow 2H_e(a^3\sum_u^+) + h\upsilon$	$\sim10^9$ s^{-1}
	$H_{e2}(A^1\sum_u^+) \rightarrow 2H_e + h\upsilon$	$\sim10^7$ s^{-1}
Conversion quenching	$H_{e2}(b^1\pi_g) + H_e \rightarrow H_{e2}(b^3\pi_g) + H_e$	$k\leq10^{-11}$ cm^3/s

2.2 Elementary processes

At atmospheric pressure, some processes are much faster than the characteristic times of glow discharge development. Such processes are assumed to be instantaneous, which simplifies the reaction kinetics and reduces the number of states in the model. A list of instantaneous reactions is given in Table 1. The objective of this paper is to formulate a mathematical fluid model in such a way that the parallel plate dielectric barrier discharge configuration is employed in the one-dimensional Cartesian form.

3 1-D Parallel Plate Discharge Modeling

The simulation of the homogeneous barrier discharge is based on the continuity equations for electrons, ions, and metastable atoms and molecules, and the Poisson equation. The mobility, diffusion, excitation and ionization coefficients are calculated on the basis of the Boltzmann equation (Table 2). The interaction between plasma and electrodes is described by boundary conditions.

4 Mathematical Models

The finest theoretical description of the particles behavior which characterizes the functioning of an electrical discharge requires the resolution of the kinetics equations as a whole (frequency called equation of discharge particle conveyance) associated at each one of these particles.

Fundamental equation rendering account of the space and temporal evolution of particles density is the equation of continuity that globally takes the same form for electrons and ions. We get the following equations:

For the electrons:

$$\frac{\partial ne(\vec{r},t)}{\partial t} + \frac{\partial(\vec{w}_e(\vec{r},t)n_e(\vec{r},t))}{\partial \vec{r}} - \frac{\partial}{\partial \vec{r}}\left[\vec{D}_e(\vec{r},t)\frac{\partial n_e(\vec{r},t)}{\partial \vec{r}}\right] = s_e(\vec{r},t) \quad \ldots (1)$$

For the ions:

$$\frac{\partial ni(\vec{r},t)}{\partial t} + \frac{\partial(\vec{w}_i(\vec{r},t)n_i(\vec{r},t))}{\partial \vec{r}} - \frac{\partial}{\partial \vec{r}}\left[\vec{D}_i(\vec{r},t)\frac{\partial n_i(\vec{r},t)}{\partial \vec{r}}\right] = s_i(\vec{r},t) \quad \ldots (2)$$

For the excited particles:

$$\frac{\partial n_m(\vec{r},t)}{\partial t} - \frac{\partial}{\partial \vec{r}}\left[\vec{D}_m(\vec{r},t)\frac{\partial n_m(\vec{r},t)}{\partial \vec{r}}\right] = S_m(\vec{r},t) \quad \ldots (3)$$

which permit to determine the space temporal evolution of the electronic and ionic densities subject to the knowledge of the running back speed, diffusion coefficient and frequencies of ionization of each charged particle.

The three aforementioned equations are named convection-diffusion equations. They are composed of the term convective (of the 1st rank with regard to the space shunted) and the term of diffusion (of the 2nd rank with regard to the space shunted).

In glow discharge, the space charge due to the ions and electrons presence is sufficient to distort the geometrical electric field. This phenomenon should be described by coupling the equations of electric and ionic conveyance with the equation of Poisson for the electric field, the equation of Poisson is written as:

$$\vec{\nabla}\varepsilon_r E = \frac{e}{\varepsilon_0}(n_i - n_e - n_n) \quad \ldots (4)$$

The equation of Boltzmann is coupled with to the one of Poisson from an auto coherent electrical model of the discharge.

5 Numerical Model

The applied voltage is:

$$V_a(t) = V_0 \sin(\mathrm{wt}) \quad \ldots (5)$$

with ω the applied angular frequency, V_0 the maximum amplitude with the root mean square voltage in this case of study being V_{rms} = 5 kV and the applied frequency f = 5 kHz.

Due to the accumulation of electric charges over the dielectric surface, a kind of "memory voltage" is developed, given by:

$$v_m(t) = \frac{1}{C_{ds}} \int_{t_0}^{t} I(t')\mathrm{d}t' + v_m(t_0) \quad \ldots (6)$$

Here, C_{ds} is the equivalent capacitance of the discharge (in fact, C_{ds}=ε_0 ε_r S/d). We used ε_r=100, a typical value for dielectric ceramics with interest in this specific device.

The actual voltage applied to the gas V_g is obtained with the relation:

$$V_g(t) = V_a(t) + V_m(t) \quad \ldots (7)$$

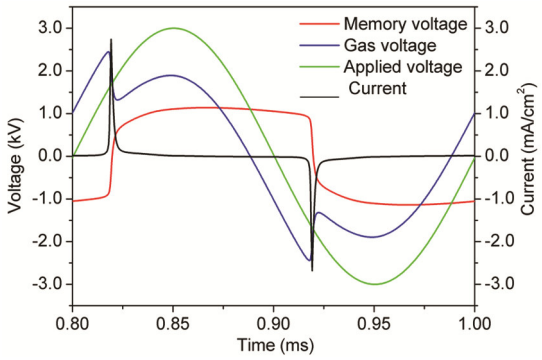

Fig. 2 — Variations of applied voltage, gap voltage memory voltage and discharge current I during one cycle[28]

The discharge (Fig. 2) is in a stationary state since it is made of a succession of identical transient discharges which occur at each half cycle of the applied voltage. The shape of the discharge current is exactly the same from one period to the next.

Although the discharge is in a stationary state and seems to have a glow behavior, we are not sure that it presents all the characteristics of glow discharges.

6 Macroscopic Approach (fluid models)

The solution developed for using this approach is designed for uniform glow-type discharges at ambient pressure. The goal of the simulation is to gain insight into key physical processes in the discharge and examine trends in the key parameters. The general form of the equations, for a species k, is shown below[29]:

$$\frac{dn_k}{dt} + \nabla.\Gamma_k = S_k - L_k \quad \ldots (8)$$

$$\Gamma_k = \frac{q_k}{|q_k|}\mu_k n_k E - D_k \nabla n_k \quad \ldots (9)$$

$$\nabla^2 \emptyset = \frac{\rho}{\varepsilon} \quad \ldots (10)$$

$$S_{e\ \mathrm{or}\ i} = \alpha_{\mathrm{io}}(E) n_0 \mu_e n_e |E| + k_{em}(E) n_e n_m + k_{pm} n_m n_p \quad \ldots (11)$$

$$L_{e\ \mathrm{or}\ i} = 0 \quad \ldots (12)$$

$$S_m = \alpha_{ex}(E) n_0 \mu_e n_e |E| \quad \ldots (13)$$

$$L_m = n_m(k_{em}(E) n_e + k_{pm} n_p + k_m \quad \ldots (14)$$

The system of equations provides a closed system for the calculation of electric potential and the production of key species. Electrons, ions, and key

neutral species are tracked in order to accurately determine the discharge behavior. Normally, neutral species are only important as a source of ionization for stagnant discharges, but for high pressure discharges containing inert gases such as helium or argon, Penning ionization and metastable quenching can be important reactions. According to the simulation developed by Novak and Bartnikas, the boundary conditions at the anode for the particles are[30]:

$$\frac{\partial n_e}{\partial Z} = n_i = n_m = 0 \quad \ldots (15)$$

For the cathode, the boundary conditions for the particles are[31] :

$$\frac{\partial n_i}{\partial Z} = n_m = 0 \quad \ldots (16)$$

$$\Gamma_e = \gamma_i \Gamma_i \quad \ldots (17)$$

The boundary conditions for the voltage depend on the information available about the discharge. The boundary conditions can be simple Dirichlet conditions. If the barrier voltage is unknown, then a more complicated boundary condition is required relating electric field to surface charge and the flow of current to the electrode. The discretization of the space is shown in (Fig. 3).

The scalar parameters such as density (n_k) and voltage (V) are taken as cell centered and vector properties such as electric field and velocity are taken at cell boundaries. Since the discharge is stagnant and ionization fraction is extremely small (<10%), the background population of ground state neutral particles (n_0) is assumed to be constant. The background population of impurities (n_p) is also assumed constant. In order to solve the system of non-linear differential equations, the relative contribution of diffusion term and convection term is important. For the metastable particles, diffusion is the only mechanism for the particle transport. For the ions and electrons, convection is the dominant mechanism for particle transport.

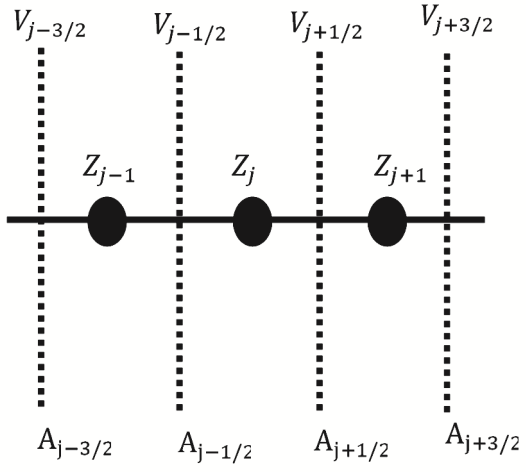

Fig. 3 — Grid for Finite Difference (1D)

$$\left|D_k \frac{\partial n_k}{\partial z}\right| \ll \left|n_k \mu_k \frac{\partial \emptyset}{\partial z}\right| \quad \ldots (18)$$

Or

$$\frac{\left|D_k \frac{\partial n_k}{\partial z}\right|}{n_k \mu_k} \ll \left|\frac{\partial \emptyset}{\partial z}\right| \quad \ldots (19)$$

6.1 Discretization of the convergence equations

Generally, we cannot solve the heavily coupled systems, constituted of the first two instants of Boltzmann's equation and of Poisson's one in a simple and direct manner. The problem is then to draw as near as necessary the exact values to the solution. The chosen method is the method of the finished differences according to the diagram of Sharfetter and Gummel[32] for the developed conveyance at the lead for semi-conductors modeling.

6.2 Discretization of the Density of the Charged Particles and of the Flux

The first step to couple the charged particle continuity equations to the Poisson equation is to discretized the charged particle continuity equations.

Known values of electron density and ion density are used for the diffusion term, source term, and loss term. For the convective term, the derivative of voltage is unknown and the charged particle density is known using the donor cell approach. The time derivative is explicitly differenced in time. The differencing scheme is first order accurate in time and space.

$$\frac{n_{k,j}^{t+\Delta t} - n_{k,j}^{t}}{\Delta t} \Delta z \pm \mu_k \left\{ n_{k,j+1/2}^{t} \frac{\emptyset_{j+1}^{t+\Delta t} - \emptyset_{j}^{t+\Delta t}}{\Delta z} - n_{k,j-1/2}^{t} \frac{\emptyset_{j}^{t+\Delta t} - \emptyset_{j-1}^{t+\Delta t}}{\Delta z} \right.$$

$$= \left(S_{k,j} - L_{k,j}\right)\Delta z + \left\{ D_{k,j+1/2}^{t} \frac{n_{k,j+1}^{t} - n_{k,j}^{t}}{\Delta z} - D_{k,j-1/2}^{t} \frac{n_{k,j}^{t} - n_{k,j-1}^{t}}{\Delta z} \right. \quad \ldots (20)$$

The result of the discretization is the charge particle continuity equations is three unknowns; the electron density, ion density, and potential at position z_j. The diffusion coefficient of the ions is constant (D_i=0.354 cm^2 s^{-1}) and the electron diffusion coefficient is a function of electric field.

$$D_e(E) = \begin{cases} 5.43 \times 10^3 \frac{|E|}{3040} \text{cm}^2\text{s}^{-1} \; E \leq 3040 \text{ vcm}^{-1} \\ 5.43 \times 10^3 \text{ cm}^2\text{s}^{-1} \end{cases} \quad \ldots (21)$$

With the electron and ion continuity equations discretized, the Poisson equation is discretized assuming all quantities are unknown.

$$\frac{-1}{q_c}\left[\frac{\emptyset_{j+1}^{t+\Delta t}-2\emptyset_j^{t+\Delta t}+\emptyset_{j-1}^{t+\Delta t}}{\Delta z^2}\right] = n_{i,j}^{t+\Delta t} - n_{e,j}^{t+\Delta t} \quad \ldots (22)$$

The discretized continuity equations are explicitly solved for the particle density for node *j*. The result of the continuity equations is substituted into the discretized Poisson equation. The source and loss terms cancel since ions and electron are ionized and recombine in the same reactions. After the substitution, the only current time variable in the discretized Poisson equation is the electric potential. The potential and associated coefficients are moved to the left side of the equation.

$$\begin{aligned} &a_1\emptyset_{j+1}^{t+\Delta t} - (a_1+a_2)\emptyset_j^{t+\Delta t} + a_2\emptyset_{j-1}^{t+\Delta t} \\ &= n_{i,j}^t - n_{e,j}^t + D_i\Delta t\left[\frac{n_{i,j+1}-2n_{i,j}+n_{i,j-1}}{\Delta z^2}\right]^t \\ &+\Delta t\left\{D_{e,j+1/2}^t\frac{n_{e,j+1}^t-n_{e,j}^t}{\Delta z^2} - D_{e,j-1/2}^t\frac{n_{e,j}^t-n_{e,j-1}^t}{\Delta z^2}\right\} \end{aligned} \quad \ldots (23)$$

Where

$$a_1 = \frac{-1}{q_c} - \frac{\Delta t}{\Delta z^2}\left[\mu_i n_{i,j+\frac{1}{2}}^t + \mu_e n_{e,j+\frac{1}{2}}^t\right] \quad \ldots (24)$$

$$a_2 = \frac{-1}{q_c} - \frac{\Delta t}{\Delta z^2}\left[\mu_i n_{i,j-1/2}^t + \mu_e n_{e,j-1/2}^t\right]$$

The particle density located at *j*±½ is evaluated using the donor cell approach.

$$\begin{aligned} n_{k,j+\frac{1}{2}}^t &= \begin{cases} n_{k,j}^t \; v_{k,j+1/2}^t > 0 \\ n_{k,j+1}^t \; v_{k,j+1/2}^t < 0 \end{cases} n_{k,j-\frac{1}{2}}^t \\ &= \begin{cases} n_{k,j-1}^t \; v_{k,j-1/2}^t > 0 \\ n_{k,j}^t \; v_{k,j-1/2}^t < 0 \end{cases} \end{aligned} \quad \ldots (25)$$

where,

$$v_{k,j\pm1/2}^t = \mp\mu_k \left.\frac{\partial\emptyset^t}{\partial z}\right|_{j\pm1/2} \quad \ldots (26)$$

The discrete Poisson equations form a linear system of equations taking the form $\bar{A}\vec{\emptyset} = \vec{b}$. The coefficient matrix $\bar{A}$ is tri-diagonal. With the voltage known at every node in space, the metastable population is calculated using the electric potential. The metastable continuity equation is differenced differently than the electron and ion continuity equations.

$$\begin{aligned} &\frac{n_{m,j}^{t+\Delta t}-n_{m,j}^t}{\Delta t}\Delta z - D_m\left\{\frac{n_{m,j+1}^{t+\Delta t}-n_{m,j}^{t+\Delta t}}{\Delta z} - \frac{n_{m,j}^{t+\Delta t}-n_{m,j-1}^{t+\Delta t}}{\Delta z}\right\} \\ &+n_{m,j}^{t+\Delta t}\left[k_{em}\left[\left.\frac{\partial\emptyset}{\partial z}\right|_j^{t+\Delta t}\right]n_{e,j}^t + k_{pm}n_p + \right. \\ &\left. k_{rm}\right]\Delta z = S_{m,j}^t\Delta z \end{aligned} \quad \ldots (27)$$

The system of discrete metastable continuity equations is linear and tri-diagonal. Unless otherwise denoted, the coefficients in the source and loss terms are constant. The electric potential is current time and the electron density is old time.

$$\mathrm{S_{m,j}^t} = \alpha_{\mathrm{ex}}(\mathrm{E^{t+\Delta t}})\mathrm{n_0}\mu_\mathrm{e}\mathrm{n_e^t}\left|\mathrm{E^{t+\Delta t}}\right| \quad \ldots (28)$$

where,

$$\alpha_{ex}n_0(E) = \begin{cases} 0 \; cm^{-1} \; E \leq 2280 \; Vcm^{-1} \\ 1.54 \times (|E| - 2280)^{0.6} \; cm^{-1} \; E > 2280 \; Vcm^{-1} \end{cases} \quad \ldots (29)$$

And

$$k_{em}(E) = \begin{cases} 0 \; cm^{-1} \; E \leq 380 \; Vcm^{-1} \\ 3.03 \times 10^{-9} \times (|E| - 380)^{0.4} \; cm^{-1} \; E > 380 \; Vcm^{-1} \end{cases} \quad \ldots (30)$$

where,

$$E^{t+\Delta t} = -\frac{\partial \emptyset^{t+\Delta t}}{\partial z} \quad \ldots (31)$$

The discrete metastable continuity equation produces a linear tri-diagonal system of the form $\bar{A}.\vec{n}_m^{t+\Delta t} = \vec{b}$. The linear system is solved using the Thomas algorithm. With the current time metastable density and current time electric potential, the electron density is calculated directly. The source term for the electron continuity equation is below[33].

$$S_{e,j}^{t} = \alpha_{io}\left[\frac{\partial \emptyset}{\partial z}\Big|_j^{t+\Delta t}\right] n_0 \mu_e n_{e,j}^{t} \left|\frac{\partial \emptyset}{\partial z}\Big|_j^{t+\Delta t}\right| + k_{em}\left[\frac{\partial \emptyset}{\partial z}\Big|_j^{t+\Delta t}\right] n_{e,j}^{t} n_{m,j}^{t+\Delta t} + k_{pm} n_{m,j}^{t+\Delta t} n_p \quad \ldots (32)$$

where,

$$\alpha_{io} n_0(E) = \begin{cases} 0\ cm^{-1}\ E \le 2280\ Vcm^{-1} \\ 5.32 \times 10^{-5} \times (|E| - 2280)^{1.5}\ cm^{-1}\ E > 2280\ Vcm^{-1} \end{cases} \quad \ldots (33)$$

The loss term is zero for the electron and ions since charged particles are lost dominantly though convection and diffusion, not recombination. The ion density is the final unknown current time quantity. The ion density is directly calculated using all the other current time quantities. The source term for the ions is below.

$$S_{e,j}^{t+\Delta t} = \alpha_{io}\left[\frac{\partial \emptyset}{\partial z}\Big|_j^{t+\Delta t}\right] n_0 \mu_e n_{e,j}^{t+\Delta t} \left|\frac{\partial \emptyset}{\partial z}\Big|_j^{t+\Delta t}\right| + k_{em}\left[\frac{\partial \emptyset}{\partial z}\Big|_j^{t+\Delta t}\right] n_{e,j}^{t+\Delta t} n_{m,j}^{t+\Delta t} + k_{pm} n_{m,j}^{t+\Delta t} n_p \quad \ldots (34)$$

With all the quantities updated to current time, the scheme is advanced to the next time step. To ensure the time advancement is numerically stable there are some limitations on the size of the time step relative to the space step, speed of the particles, and the diffusion coefficient of the particles. The Fourier Modulus determines the numerical stability limit of conduction/diffusion equations. The Courant limit determines the numerical stability limit of convective equations. The limit of numerical stability for a mixed equation is determined by both limits.

$$2.\frac{D_k \Delta t}{\Delta z^2} + \frac{|v_k|_{max} \Delta t}{\Delta z} < 1 \quad \ldots (35)$$

Since the spatial step and time step are constant for all species, the particle with the largest speed and largest diffusion coefficient determines the numerical stability of the system. The electrons have both the largest speed and the largest diffusion coefficient so they determine the numerical stability of the system.

7 Results and Discussion

The mobility and diffusion coefficient used are the same as those in[35-38]. The photo–ionization contribution is not taken into account in this model. As the initial condition, we assume that the electron density and the atomic ion density are equal to each other and uniformly distributed in the discharge region $n_e(r,0) = n_i(r,o) = 10^7$ cm^{-3}, while the molecular ion density and the excited atom density are both 10^2 cm^{-3}. The spacing between the two electrodes is 5 mm; a sinusoidal voltage is externally applied to the inner electrode, its amplitude, frequency and temperature are 4 kv, 4 kHz and 300 K, respectively.

Figures 4 and 5(a, b) show the temporal evolution of the total discharge current, the gas voltage during a typical cycle and current density. It can be seen that there is one current peak in each half cycle of the applied voltage. Different from the parallel-plate configuration, the current peak in various half periods loses its original shape. The current maximum of 2.3 mA in the first half is different from the second, which is only -7.1 mA. In addition, the pulse width of the discharge current in the latter half period is wider than that in the former (Fig. 5(a)). It is due to the fact that in the first half, the discharge cathode is the outer electrode with a big radius so that the volume of ionization region in the cathode sheath is also very large, leading to a strong current gathering; while in the latter half period, the discharge cathode is the inner wire electrode with a much smaller radius. Although in the latter case the sheath electric field is much stronger than that in the former, the volume of the ionization region is however so small that it leads to a smaller current peak. The blue line in Fig. 4 represents the time evolution of the gas voltage with

the applied voltage during a typical cycle. At the initial moment, the applied voltage is zero, and the gas voltage is not zero but equal to the memory voltage produced by the charged particles accumulated on the dielectric. As the applied voltage rises, the gas voltage increases until it reaches the breakdown voltage. Then the gas is punctured and discharge starts. Meanwhile, the charges accumulated on the dielectric produce a reverse electric field,

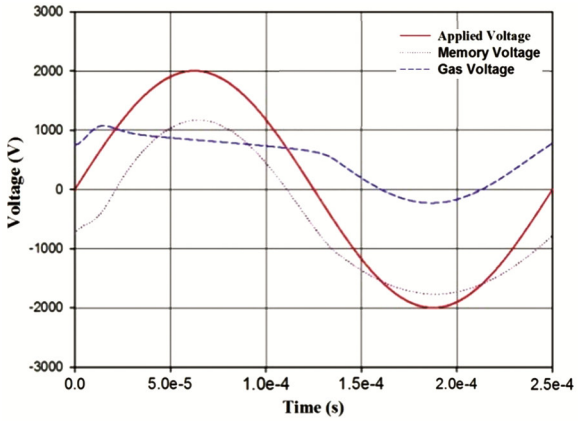

Fig. 4 — Evolution of the gas voltage in typical cycle

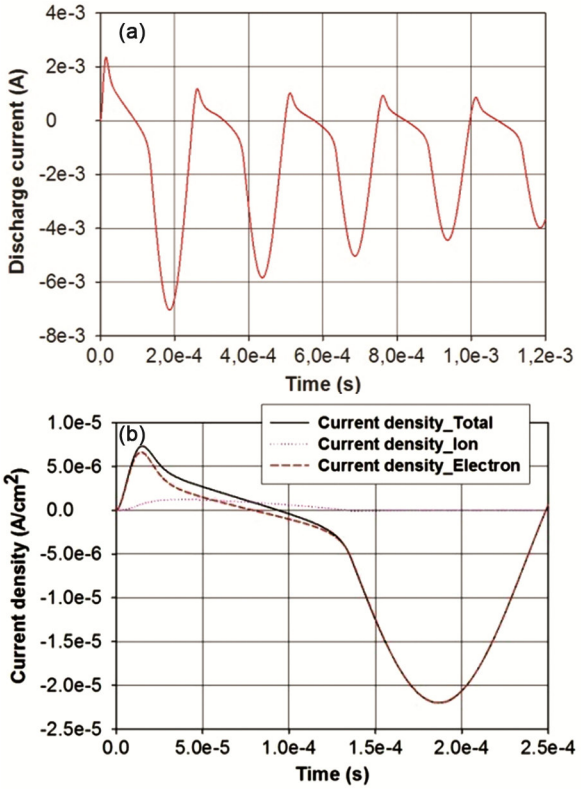

Fig. 5 — (a) Evolution of the total discharge current in typical cycle and (b) evolution of the current density in typical cycle

making the gas voltage drop and leading to a termination of the gas discharge. In the latter half period, due to the reversal of the applied voltage, the electric field produced by the accumulated charges has the same direction as the applied field, so it reduces the threshold applied voltage for starting the next discharge. Furthermore, since the breakdown during the latter half period happens in the cathode sheath near the inner wire electrode, where the electric field is strong, correspondingly it is easier to puncture, and therefore the breakdown voltage in the latter half period is lower than that in the former half period. As a result of the higher discharge current during the former half period, the accumulation seed of charged particles on the dielectric barrier is fast too. Then the gas voltage drops rapidly and the discharge is suppressed quickly, and consequently the discharge current pulse is narrow. However, during the latter half period, since the discharge current is low, the accumulation speed of charged particles on the dielectric is also low. Thus the gas voltage changes slowly and its suppressing effect on discharge is small, so the current pulse is wide.

Figures 6-13 illustrate the spatial distributions of the electric field, the electron, and the ion as well as the excited atom densities in the different times.

7.1 Discharge extinction

At the beginning of the alternation, before the discharge, the inter-electrode gas space can be regarded as a capacitive voltage divider. When the voltage at the cell terminals increases, the voltage applied to the gas also increases until the electric field reaches the value required to initiate an avalanche. This particular value of the voltage of the gas is called ignition voltage. Irradiation leads to the development of an electron avalanche which propagates toward the

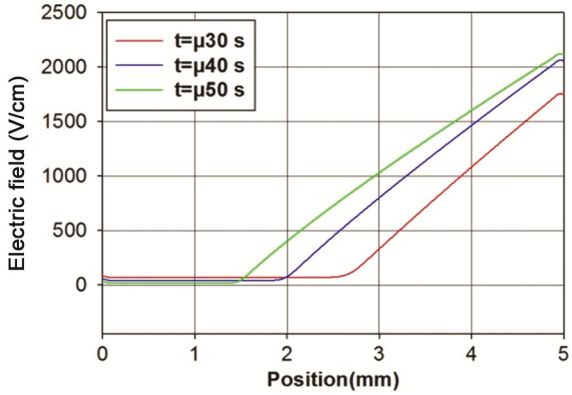

Fig. 6 — The spatial distribution of electric field (t=30, 40 and 50 μs)

anode. As the ion mobility is significantly lower than that of electrons (approximately 1000 times lower), they are accelerated with greater velocity toward the anode. They leave behind positive ions virtually immobile. The voltage of the gas is constant during this phase

The applied increasing voltage induces an increase in the electric field and the ion density slightly increases from the side of the anode and in a much more marked next to the cathode. The mobility of ions is much lower than that of the electrons and the rapid movement of electrons induces a positive space charge and causes an increase of the electric field and therefore the construction, near the cathode,

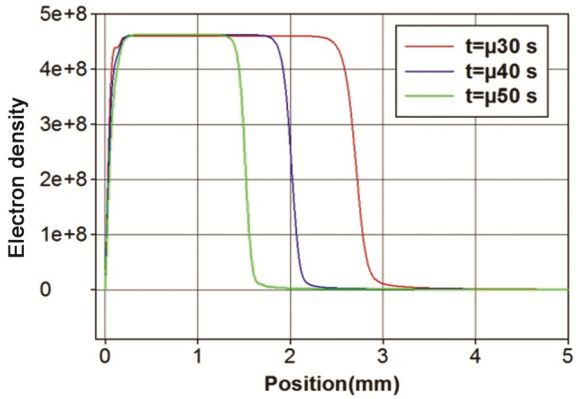

Fig. 7 — The spatial distribution of electron density (t=30, 40 and 50 μs)

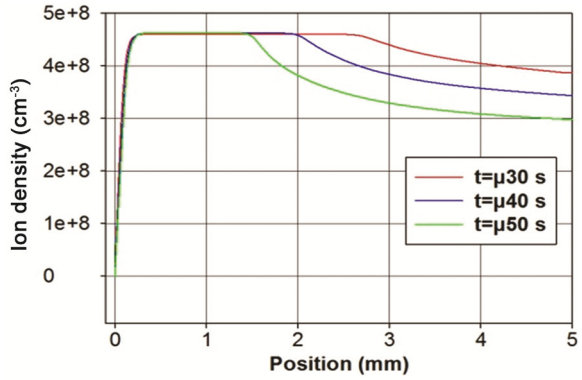

Fig. 8 — The spatial distribution of ion density (t=30, 40 and 50 μs)

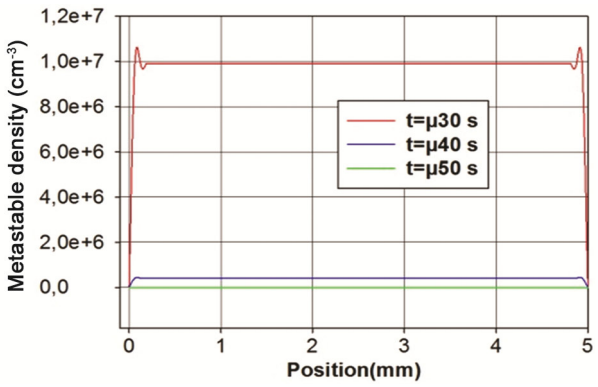

Fig. 9 — The spatial distribution of metastable density (t=30, 40 and 50 μs)

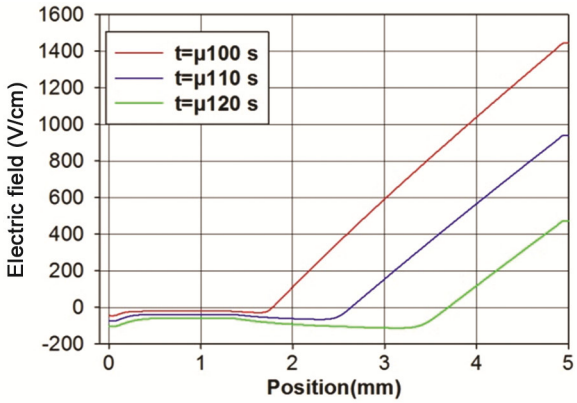

Fig. 10 — The spatial distribution of electric field (t=100,110 and 120 μs)

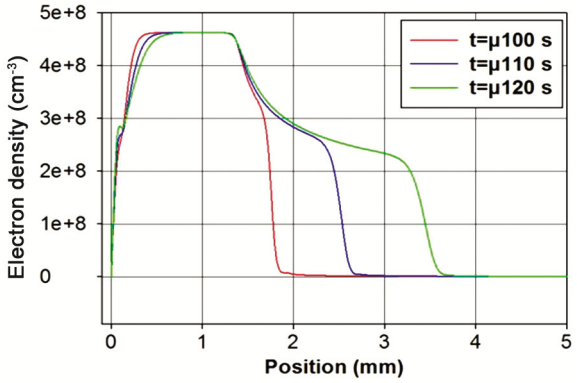

Fig. 11 — The spatial distribution of electron density (t=100,110 and 120 μs)

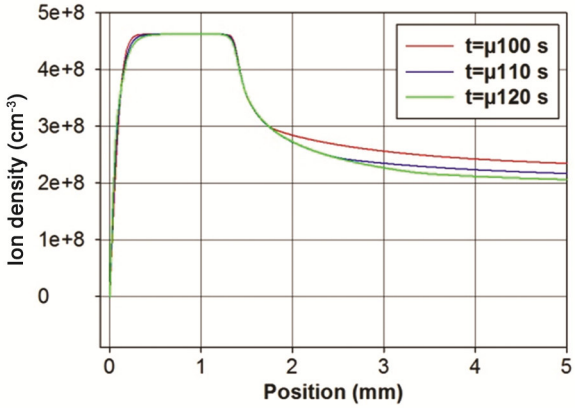

Fig. 12 — The spatial distribution of ion density (t=100,110 and 120 μs)

of a strong field area: the cathode fall. The metastable that are created by electron impact, move by diffusion. And a part of the density reaches the surface despite the low diffusion at atmospheric pressure.

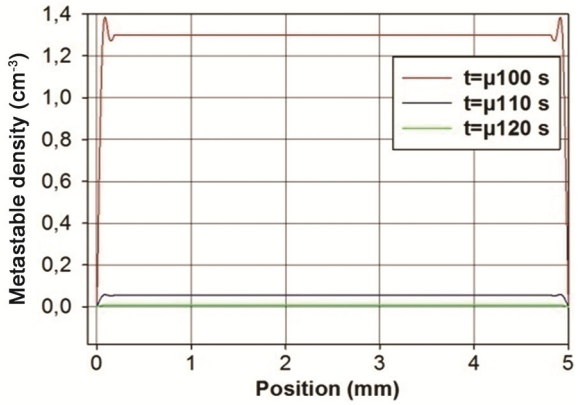

Fig. 13 — The spatial distribution of metastable density (t=100,110 and 120 µs)

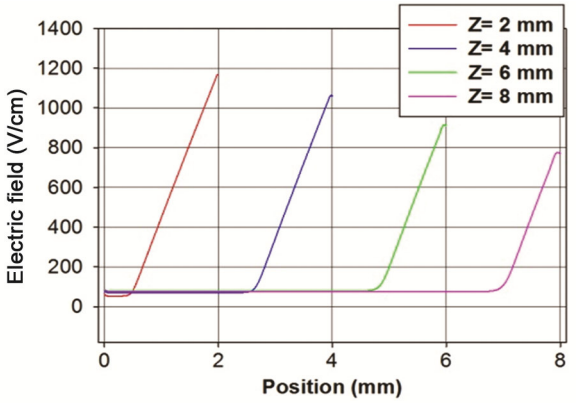

Fig. 14 — The spatial distribution of electric field (z=2, 4, 6 and 8 mm)

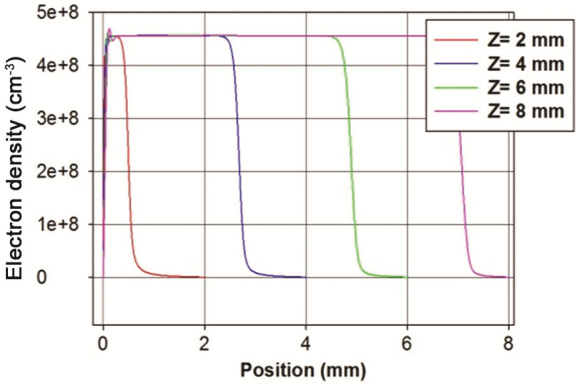

Fig. 15 — The spatial distribution of electron density (z=2, 4, 6 and 8 mm)

7.2 Priming of the discharge

Figure 14 represents the spatial variation of the electric field in the inter-electrode space, and the electron densities, ionic and metastable, which are the majority species in the discharge.

These distributions are presented at maximum of current. As we can see, the electric field to keep an almost constant value throughout the inter-electrode space. The electron density varies exponentially; such behavior corresponds to a discharge of Townsend, that is to say, a self-sustaining discharge by the emission of electrons at the cathode. The electrons are multiplied exponentially during travel from the cathode to the anode as the ion density is too low to induce a localization of the electric field. The field being substantially uniform, the value of the geometric field is strong, which makes it possible to maintain ionization. The energy transfer is maximal at the anode where the electron density is maximum. In the cathode zone the maximum value of the electric field decreases. In both zones the positive column and the anode sheath the charge densities are equal and the electric field is increasingly low. The highest values of the electron and ion densities decrease in the cathode zone but remain constant in the positive column because the charged particle (electron and ion) are trapped within the positive column.

Metastable densities remain constant because they do not depend on electric field. These species, being neutral, their movement is determined by the distribution, that is to say the concentration gradient.

7.3 Discharge ignition

In Fig. 15, we can see the spatial distributions of the electric field and electron densities, ionic and metastable in stable condition. At this time the plasma is already formed in the cathode sheath, the plasma formed near the anode, the densities of particles in plasma increased in function of time. The dynamics of the ionization process in the active phase of the discharge formation depends on the densities of charges accumulated in the discharge volume[39-40].

It is noted that the electric field decreases when the voltage of the gas decreases. This decrease can no longer be done quickly to the cathode side due to the high ion density in this area and decrease of the electric field at the anode induces a displacement of the electrons near the electrode which will become the new anode (right) and the ions approach the new cathode.

The maximum of the metastable density is very low, but these species remain constant over the entire electrode surface area since they are independent of the electric field.

7.4 Parameter variation

7.4.1 Effect of the inter electrode distance

From this study, we can define three ranges of variation of the inter-electrode distance where the discharge characteristics are identical. For distances between 2 mm and 8 mm, the glow discharge guard structure and the decrease or increase of the inter-electrode distance leads to a reduction or an increase in the extent of the positive column. Below 3 mm, the positive column disappears completely and the remaining areas are compressed: the discharge becomes unstable and begins to have a particular behavior. For inter electrode distance above 8 mm, the positive column reaches a critical size and the applied electric field is high enough to ensure self-maintain of the discharge.

7.4.2 Excitation frequency

Figures 16 and 17 represent the influence of the frequency in the spatial variation of the electric field and the densities of the particles. Any increase in the frequency induces an increase in the electron density and we notice that when the electric field is very small electron density is quite high because electrons travel time is very low. Note that under certain conditions, the electron density of the initial avalanche can be relatively large. Secondary avalanche from the cathode can reach the tail of the initial avalanche even before it reaches the anode. It is difficult to determine the boundary between these two phases, from the evolution of current. Although the sampling frequency is 3 kHz, do not allow to obtain simultaneously a wide range of time and a high sampling frequency, a bit marked peak was able to be masked.

7.4.3 Effect of the applied voltage

The ignition voltage under our conditions is the maximum value of the voltage of inter-electrode space (Figs 18 and 19). The breakdown voltages derived from the Paschen curves. They are given for the breakdown in pure helium between two planar metal electrodes. These voltages correspond to breakdown criteria in continuous operation in a homogeneous field. According to Kogelschatz *et al*, the starting voltage for the inter-electrode space, limited by one or two dielectric layers, is substantially equal to that of a device provided with two metal

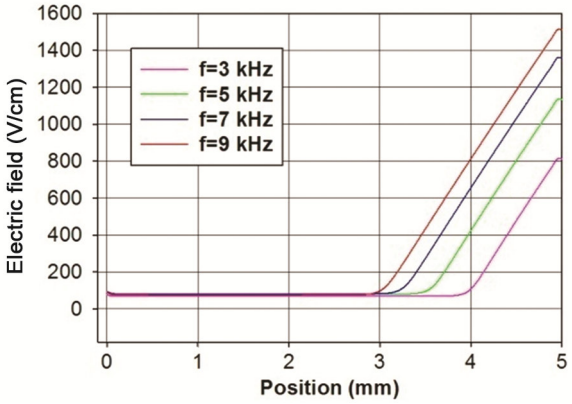

Fig. 16 — The spatial distribution of electric field (*f*=3, 5, 7 and 9 kHz)

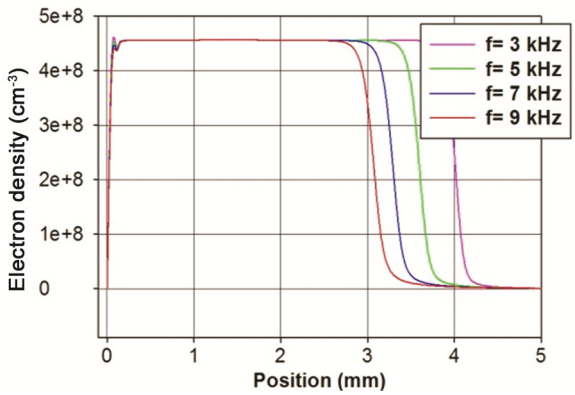

Fig. 17 — The spatial distribution of electron density (*f*=3, 5, 7 and 9 kHz)

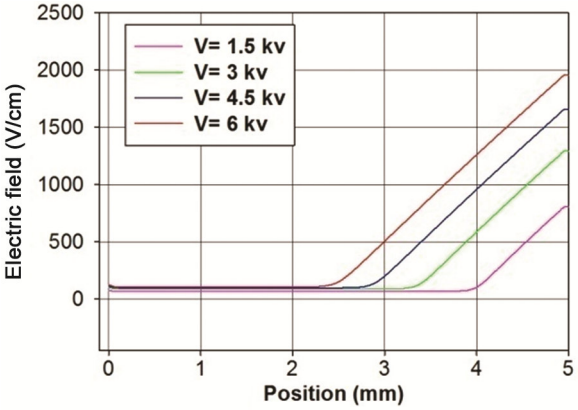

Fig. 18 — The spatial distribution of electric field (*V*=1.5, 3, 4.5 and 6 kv)

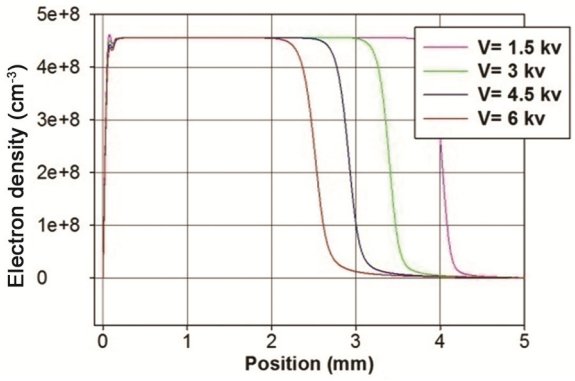

Fig. 19 — The spatial distribution of electron density (V=1.5, 3, 4.5 and 6 kv)

electrodes at 4 kHz and the lower filling pressures (P <300 Torr), our voltage values are 20% higher than those derived from the Paschen curves. For pressures higher than 500 Torr, the apparent starting voltage, under our conditions, is less than that deduced from the Paschen curves. In addition, 4 kHz, it is always less than that obtained from the Paschen curves. Which means that high frequency electrical breakdown process in the DBD is linked to the pre-ionization effect, due to the fact that the charges are not completely removed, which is responsible for the decrease of the breakdown voltage.

It is noted that when the applied voltage increases, the thickness of the cathode sheath increases. This region is characterized by an electron density which becomes increasingly smaller with increasing the applied voltage, this is explained by the fact that the increase of the applied voltage leads to an increase of the electric field; the latter has the effect of increasing the velocity of charged particles, in particular electrons are much lighter than ions. The electron density in positive column is the same regardless of the applied voltage.

8 Conclusions

Based on the one-dimensional and self-consistent fluid model, the characteristics of the dielectric barrier glow discharge in pure helium at atmospheric pressure generated between two coaxial electrodes is investigated numerically. In calculation, we have considered the elementary ionization and excitation processes in pure helium. Under the drift-diffusion approximation, by solving the one-dimensional continuity equations for electrons, ions and excited atoms, together with the current conservation equation, the simulation results show the spatial-temporal distributions of the electric field and the electron, ion and excited atom densities, as well as the time evolutions of the discharge current and the gas voltage. At maximal discharge current, there obviously exist the cathode fall, the negative glow region and the positive column, similar to the APGD with the dielectric barrier between parallel-plate electrodes.

It is unlikely that surface charging of the dielectric electrodes would play a predominant role in the tendency for the rate of current rise to increase with frequency, since the particular behavior is manifested with both the metallic and dielectric electrode gaps. For example, in going from 2 to 10 kHz, the rate of current rise with the two-metallic electrode gap increases from 0.19 to 0.77 mA/μs screw-have-screw 0.02 to 0.67 mA/μs for the two-dielectric electrode gap. The development of space charge cannot be attributed to overvoltage effects, since no significant increase in breakdown voltage with increasing frequency is observed. A more plausible explanation that can be advanced at this time would appear to be that with rising frequency, increasingly less time becomes available for the accumulated ions to be dispersed from the vicinity of the cathode region. However, further experimentation is necessary to clarify the details of this mechanism.

References

1 Roth J R, *Ind Plasma Eng*, 2 (1995) 55.
2 Massines F, Gherardi N & Naudé N, *Plasma Phys Control Fusion*, 47 (2005) 577.
3 Luo H Y, Liang Z & LV B, *Appl Phys Lett*, 91 (2007) 221504.
4 Roth J R, Sherman D M & Wilkinson S P, *Boundary Layer flow Control with a one Atmosphere Uniform Glow Discharge*, AIAA paper 98-0328, 36th AIAA aerospace Sciences Meeting and Exhibit, Reno, NV, 1998 .
5 Corke T C, Jumper E J, Post M L, Orlov D & Mclaughlin T, *Application of Weakly-Ionized Plasmas as wing flow-Control Devices*, AIAA paper 2002-0350, 41st Aerospace Sciences Meeting and Exhibit, Reno, NV, 2003
6 Kim Y, Kang W S, Park J M, Hong S H, Song Y H & Kim S J, *IEEE Trans Plasma Sci*, 32 (2004) 18.
7 Roth J R, Rahel J, Dai X & Sheman D M, *J Phys D: Appl Phys*, 38 (2005) 555.
8 Shenton M J & Stevens G C, *J Phys D: Appl Phys*, 34 (2001) 2761.
9 Golubovskii Y B, Maiorov V A, Behnke J & J Behnke F, *J Phys D: Appl Phys*, 36 (2003) 39.
10 Tendero C, Tixier C, Tristant P, Desmaison J & Leprince P, *Spectrochim Acta B*, 61 (2006) 2.
11 Massines F, Ségur P, Gherardi N, Khamphan C & Ricard A, *Surf Coat Technol*, 8 (2003) 174.
12 Webb M R, Andrade F J & Hieftje G M, *Anal At Spectrom*, 22 (2007) 775.

13 Montie T C, Kelly-Wintenberg K & Roth J R, *IEEE Trans Plasma Sci*, 28 (2000) 41.
14 Yang X, *Plasma Sources Sci*, 19 (2005) 314.
15 Massines F, Messaoudi R & Mayoux C, *Plasma Polym*, 3 (1998) 43.
16 Singh K P, Roy S & Gaitond D V, *Modeling of Dielectric Barrier Discharge Plasma Actuator with Atmospheric Air Chemistry*, AIAA paper 2006-3381, 37th AIAA Plasma dynamics and lasers conference, San Francisco, CA, 2006.
17 Gadri R B, *IEEE Trans Plasma Sci*, 27 (1999) 36.
18 Golubovskii Yu B, Mairov V A, Behnke J F, Tepper J & Lindmayer M, *J Phys D: Appl Phys,* 37 (2004) 1346.
19 Anderson C, Hur M & Zhang P, *J Appl Phys,* 96 (2004) 1835.
20 Nersisyan G & Graham W G, *Plasma Sources Sci Technol,* 13 (2004) 582.
21 Hagelaar G J M, *Ph. D. Thesis*, Technische Universiteit Eindhoven, 2000.
22 BOLSIG+,freeware,wwwsiglokinemacom/bolsightm.
23 Deloche R, Monchicourt P, Cheret M & Lambert F, *Phys Rev,* 13 (1976) 1140.
24 Stevefelt J, Pouvesle J M & Bouchoule A, *J Chem Phys,* 76 (1982) 4006.
25 Collins C B, Hicks H S, Wells W E & Burton R, *Phys Rev A*, 6 (1972) 1545.
26 Rauf S & Kushner M J, *J Appl Phys,* 85 (1999) 3460.
27 Pouvesle J M, Bouchoule A & Stevefelt J, *J Chem Phys,* 77 (1982) 817.
28 Massines F, Gherardi N, Naudé N & Ségur P, *Plasma Phys Control Fusion*, 47 (2005) 577.
29 Pal U N, Gulati P, Kumar N, Srivastava V & Prakash R, *IEEE Trans Plasma Sci*, 40 (2012) 1356.
30 Novak J P & Bartnikas R, *J Phys D: Appl Phys*, 21 (1988) 896.
31 Frank L, Robert H S, El-Habachi A & Schoenbach K H, *J Phys D: Appl Phys*, 33 (2000) 2268.
32 Scharfetter D L & Gummel H K, *IEEE Trans Electron Dev*, 16 (1969) 64.
33 Mangolini L, Anderson C, Heberlein J & Kortshagen U, *J Phys D: Appl Phys*, 37 (2004) 1021.
34 Roy S & Gaitonde D V, *Modeling Surface Discharge Effects of Atmospheric RF on Gas Flow Control*, Proceeding 43rd AIAA aerospace Sciences meeting, 160 (2005) 10-13.
35 Shi J J & Kong M G, *J App Phys*, 94 (2003) 5504.
36 Pal U N, Sharma A K, Soni J S, Kumar S, Khatun H, Kumar M, Meena B L, Tyagi M S, Lee B-J, Iberler M, Jacoby J & Frank K, *J Phys D: Appl Phys*, 42 (2009) 045213.
37 Pal U N, Gulati P, Kumar N, Kumar M, Tyagi M S, Meena B L, Sharma A K & Prakash R, *IEEE Trans Plasma Sci*, 39 (2011) 1475.
38 Gulati P, Pal U N, Prakash R, Kumar M, Srivastava V & Vyas V, *IEEE Trans Plasma Sci*, 40 (2012) 2699.
39 Mankour M & Belarbi AW, *Int J Phys Sci*, 7(3) (2012) 361.
40 Mankour M, Belarbi A W & Hartani K, *Rom Rep Phys*, 65 (2013) 230.